Biochimica et Biophysica Acta 1838 (2014) 1104–1112

Contents lists available at ScienceDirect

Biochimica et Biophysica Acta

journal homepage: www.elsevier.com/locate/bbamem

Correlation of biological activity with computationally derived structural features from transmembrane hetero-dimers of HIV-1 Vpu with host factors ☆

Li-Hua Li, Wolfgang B. Fischer *

Institute of Biophotonics, School of Biomedical Science and Engineering, and Biophotonics & Molecular Imaging Research Center (BMIRC), National Yang-Ming University, Taipei 112, Taiwan

ARTICLE INFO

Article history:
Received 22 May 2013
Received in revised form 26 July 2013
Accepted 31 July 2013
Available online 13 September 2013

Keywords:
Vpu HIV-1
Membrane protein
Host factors
Molecular dynamics simulations
Docking approach

ABSTRACT

Vpu is an 81 amino acid type I integral membrane protein encoded by human immunodeficiency virus type 1 (HIV-1). It is identified to support viral release by potentially forming ion and substrate conducting channels and by modulating the function of host factors. The focus is on the interaction of the transmembrane domains of Vpu with those of host factors using a combination of molecular dynamics simulations and docking approach. Binding poses and adopted tilt angles of the dimers are analyzed and correlated with experimentally derived activity data from literature. Vpu activity is driven by dimerization with the host protein *via* its alanine rim Ala-8/11/15/19. Tight binding is shown by an almost parallel alignment of the helices in the dimers. Less parallel alignment is proposed to correlate with lower activity. This article is part of a Special Issue entitled: Viral Membrane Proteins — Channels for Cellular Networking.

© 2013 Elsevier B.V. All rights reserved.

1. Introduction

Viral channel proteins belong to the class of proteins that self-assemble into homo-oligomers enabling ion and substrate flux across the lipid membrane [1,2]. The consequence of this is an altered environment for improved reproduction of the virus. It has been shown that the mode of action of these proteins is important in the early stage of viral entry into the host, e.g. for Kcv from PBCV-1 [3], and in the later stage of the infectivity cycle, e.g. for Vpu from HIV-1 (reviewed in [4]). In the case of the viral proton conducting channel M2 from influenza A, the protein is found to be essential during the early stage as well as during the later stage, while other viral proteins need to be manufactured [5,6]. In all the stages mentioned it is rather the proton/ion flux which is thought to trigger downstream molecular mechanical events.

In recent years it has become evident that Vpu from HIV-1 is interacting with a number of host factors such as CD4, BST-2 and NTB-A (reviewed in [1]). Similarly, E5 of human papillomavirus 16 has recently been identified to release ions and substrates using fluorescent dye release essays with liposomes [7]. E5 is declared as a member of the channel forming viral proteins and is also known for its interaction with a series of host factors [8,9]. This sparks thoughts about the importance of the role of channel formation in comparison to the role of manipulating the host cell via interaction with host-factors (for Vpu see [10,11]). How these proteins 'find' their partners, and how strong the interaction to the attached host proteins must be in order to be processed further are still to be elucidated.

Vpu is an 81 amino acid type I integral membrane protein found in HIV-1 [12,13] and related chimpanzee isolate SIV_{CPZ} [14]. As an auxiliary protein it amplifies virus replication [15] (for review see [16–18]). Shortly after its discovery the mechanism of amplification has been attributed to its capability to oligomerize [19–21], to form channels within the lipid membrane [22] and to down-regulate the receptor protein CD4 [23]. In the first case channel formation was found to be solely due to the transmembrane domain (TMD) of Vpu. Randomization of the TMD of Vpu leads to an abrogation of channel activity [22]. In the second case the cytoplasmic domain was identified to be essential. In recent years more host factors have been identified such as CD317/tetherin/BST-2 [24–26], CD74 [27] and NTB-A [28] with which Vpu is supposed to interact. The consequence of the interaction is that these proteins are redirected to the ubiquitin-dependent proteasome degradation pathway. In the case of both CD317/tetherin/BST-2 [24–26,29] and NTB-A [28] the TMD of each of the membrane proteins is the target of Vpu.

NMR spectroscopic experiments of peptides corresponding to the TMD of Vpu reveal a helix which is kinked around Ile-17 [30–33]. The kink is also found in molecular dynamics (MD) simulations of the TMD when embedded into hydrated lipid bilayers and includes Ile-20 to Ser-24 [34]. The physical interaction of the TMDs of Vpu and BST-2 is confirmed by NMR spectroscopy to be driven by hydrophobic interactions between the two helices [35]. The alanine rim of Vpu allows larger residues within the TMD of BST-2, such as V-30, I-34 and L-37, to

☆ This article is part of a Special Issue entitled: Viral Membrane Proteins — Channels for Cellular Networking.

* Corresponding author at: Institute of Biophotonics, School of Biomedical Science and Engineering, National Yang-Ming University, 155, Li-Non St., Sec. 2, Taipei 112, Taiwan. Tel.: +886 2 2826 7394; fax: +886 2 2823 5460.
E-mail address: wfischer@ym.edu.tw (W.B. Fischer).

0005-2736/$ – see front matter © 2013 Elsevier B.V. All rights reserved.
http://dx.doi.org/10.1016/j.bbamem.2013.07.032

interact tightly. The alanine rim follows an AxxxAxxxA motif which is conserved among Vpu isolates [36]. This motif adds up to a series of known motifs for TMD–TMD interactions [37,38].

Computational protocols are proposed to generate dimeric and oligomeric assemblies of membrane proteins and peptides based on the TMDs using docking based screening of the interhelical interactions [39–43], (reviewed in [44]). There have been attempts to derive TMD-oligomerization by allowing full scale protein dynamics by simulating the process in a lipid bilayer environment [40,45,46].

In this study we focus on the structural features and dynamics of the TMDs of Vpu and Vpu mutants once assembled into dimers either with BST-2, CD4 or NTB-A. In each case, the TMDs are known to be the segments of the proteins relevant for their biological function. While BST-2, NTB-A and Vpu interact *via* their TMDs, for Vpu and CD4 they seem not to be the only contact point. It is investigated whether results from MD simulations can be correlated with related biological experiments. Vpu is not necessarily co-down-regulated with all host factors used in this study. It is anticipated that there has to be a structural and dynamical aspect in the interaction because Vpu needs obviously also to dissociate from the host-TMD, especially while interacting e.g. with BST-2.

This study is seen as an attempt to use the tools in a computational bioanalytical approach. The helical motif of TMDs can easily be modeled based on bioinformatics tools such as secondary structure prediction programs. Limiting the study to the TMDs is, besides the biological relevance of these domains as mentioned, also due to minimize calculation time when screening larger data sets.

2. Materials and methods

Ideal helices ($\phi = -65°$, $\psi = -39°$) of the N terminal side of Vpu (Vpu HV1H2), including the TMD of the protein as well as the TMDs of CD4, BST-2 and NTB-A were generated using the program MOE2008.10 (Molecular Operation Environment, www.chemcomp.com):

Vpu_{1-32} (Vpu)	MQPIPIVAIV[10] ALVVAIIIAI[20] VVWSIVIIEY[30] RK
Random Vpu_{1-27} (RVpu)	MIPIVIAIIL[10] AVAVQAIVIV[20] IVSWIIE
$CD4_{397-418}$ (CD4)	MALI[400] VLGGVAGLLL[410] FIGLGIFF
$BST\text{-}2_{5-27}$ (BST-2)	LLGIGI[10] LVLLIVILG[20] VPLIIF
$NTB\text{-}A_{229-249}$ (NTB-A)	FM[230] VSGICIVFGF[240] IILLLLVLA.

The sequence of RVpu was taken from [22]. The mutations of the TMD of Vpu_{1-32} are done as following A19H, A19L, A19N, A19F, A15L, A15N, A15F, W23A, I16/17/18T (I3xT), and I16/17/18V (I3xV). This four letter code is used in the text.

2.1. Preparation of the protein/lipid/water system

Proteins, uncharged at both ends, were embedded into POPC lipid bilayer patches (POPC: 16:0–18:1 diester PC, 1-palmitoyl-2-oleoyl-*sn*glycero-3-phosphocholine). Prior to protein insertion, patches of 128 lipids were equilibrated for 70 ns [34] and used for the simulations.

Individual helices and protein assemblies were inserted into the POPC bilayer patches using the MOE software package. Lipids were manually removed to avoid an overlapping with the proteins. Finally, the patches consisted of 122 lipids (6344 atoms). The protein/lipid system was hydrated with about 3655 water molecules.

All MD simulations were carried out using GROMACS 4.0.5 with the Gromos96 (ffG45a3) force field. Peptides, lipids, and the water molecules were separately coupled to a Berendsen thermostat at 310 K with a coupling time of 0.1 ps. The compressibility was set to 4.5×10^{-5} bar^{-1}. The monomers were simulated using a semi-isotropic pressure coupling scheme. Long range electrostatics was calculated using the particle-mesh Ewald (PME) algorithm with grid dimensions of 0.12 nm and interpolation order 4. Lennard–Jones and short-range Coulomb interactions were cut off at 1.4 and 0.9 nm, respectively. Water molecules were represented by the SPC model. The protein/lipid/water system was energy minimized (1000 steps steepest descents, 5000 steps of conjugate gradient) followed by a total of 1.9 ns (122 lipid patch) of equilibration MD simulation. The following equilibration protocol was used: (i) the temperature was gradually increased from 100 K to 200 K and 310 K. The system was run for 200 ps for the first two temperatures and 1.5 ns for the latter (500 ps for the patch containing 122 lipids). During these simulations the protein remained fully restraint ($k = 1000$ kJ mol^{-1}). At 310 K the restraints kept on the protein *via* the force constant k, were released in 2 steps from $k = 500$ kJ mol^{-1} nm^{-2} to $k = 250$ kJ mol^{-1} nm^{-2}. Each step was run for 1.5 ns. For the system containing 122 lipids, 2 steps ($k = 500$ kJ mol^{-1} nm^{-2} and $k = 250$ kJ mol^{-1} nm^{-2}) were used each running for 500 ps.

2.2. Assembly

The starting structure for the assembly of TMDs was the average structure over the backbone atoms of the 100 ns MD simulations. Rotational and translational motions were removed by fitting the peptide structure of each time frame to the starting structure. The program g_covar from the GROMACS-3.3.1 and 4.0.5 packages was used for the calculations [42].

The dimers were assembled using a program based on the scripting language 'scientific vector language' (SLV) of the MOE suit as reported earlier [42,43]. For energy calculations the AMBER 94 force field was used. To simulate the assembly within the lipid bilayer the dielectric constant (ε) was set as $\varepsilon = 2$. The helical backbone structures were aligned along the *z*-axis. The conformational space of the assembly was screened by keeping one helix fixed but free to rotate around its own axis while the second helix was able to move in respect to the interhelical distance, its tilt in respect to the other helix and to rotate as well around its own axis. All dimers were generated by screening the interhelical distance in steps of 0.25 Å, the tilt and rotational angles in steps of 2° and 5°, respectively. Interhelical distances were varied between 8 and 13 Å for each peptide, and the tilt was varied between ±36°. The assembly protocol usually generated about 350,000 conformers which were stored in a data base for further analysis.

Plots of the root mean square fluctuation (RMSF) of the Cα atoms of each residue as well as calculations of the tilt and kink angles were generated over the last 70 ns of the 100 ns simulation and over the entire duration of the 200 ns simulation run. The tilts and kink are measured using the coordinates of the center of mass calculated from the backbone of residues 5–8, 20–23 and 24–28.

The simulations were prepared on a DELL T7500 workstation and submitted to the National Center for High Performance Computing (NCHC), Hsinchu, TW using 24 cpu's in parallel for 168 h for the production run of 200 ns.

Plots and pictures were made with VMD-1.8.7, Origin 8.5 and Pymol.

3. Results

The helical motif of each of the TMDs of Vpu, CD4, BST-2, NTB-A, A19H, I3xT and W23A remains intact during a 100 ns MD simulation (Fig. 1A). The RMSD shows the general pattern of a rise which is plateauing off after the first ns (Fig. 1B). The RMSF values express a *w*-like shape for all the TMDs (Fig. 1C). Mutant A19H shows the highest dynamics around Ile-16 and the mutated His-19 (Fig. 1C, II) compared with the other peptides. Residues from the middle of the helix towards the C terminus exhibit a gradual increase in fluctuation for BST-2. The respective values for any mutant Vpu_{1-32} show the same trend for both RMSD and RMSF values as shown in Fig. 1 (data not shown).

While assembling the TMDs mentioned above and those of other mutant of Vpu_{1-32} with BST-2 using the docking software, the distance between the dimers ranges between 9.5 and 12.75 Å (Table 1, Suppl.

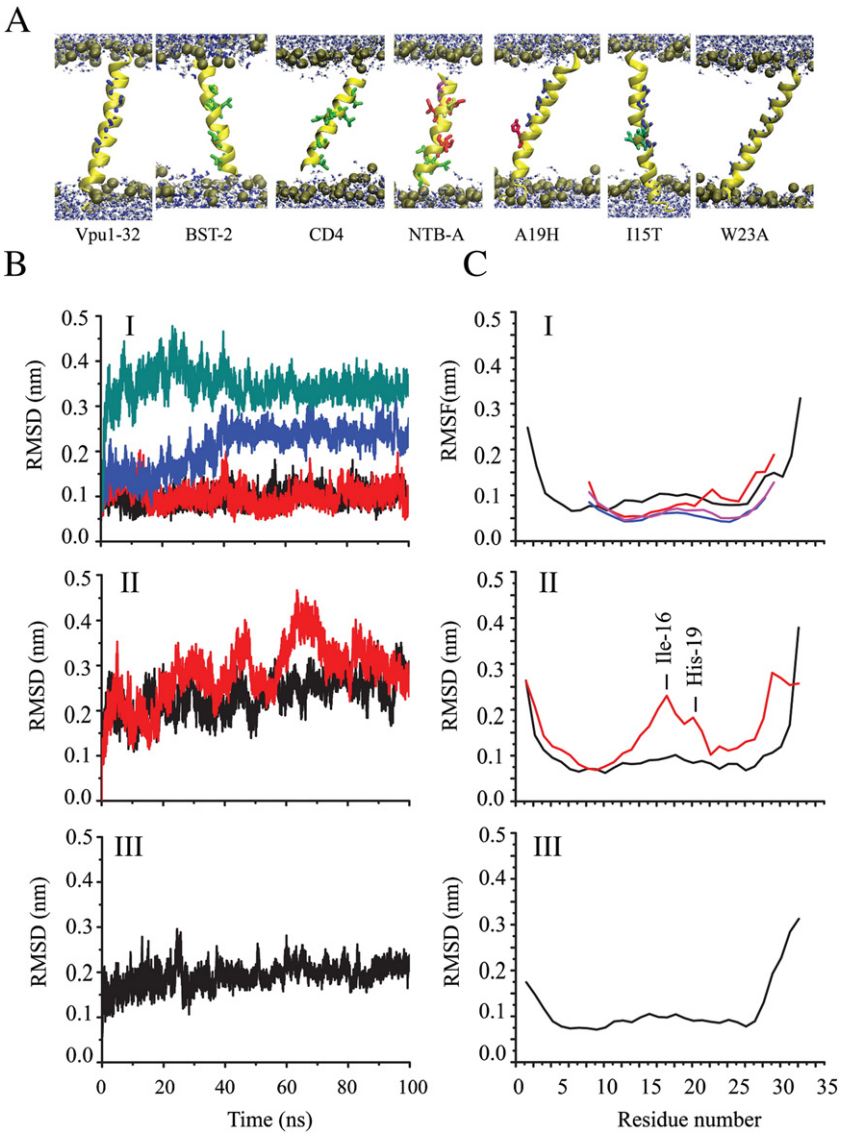

Fig. 1. Graphical representation of the individual TMDs after 100 ns MD simulation (A). The TMDs are shown from left to right Vpu, BST-2, CD4, NTB-A, A19H, I3xT, and W23A. The peptides are shown with their backbone highlighted in yellow. Amino acids are shown in stick modus and colored as the following: alanine (blue), leucine (green), isoleucine (red), histidine (dark red), cysteine (light pink), and threonine (dark green). Phosphorous atoms are shown as dark spheres to mark the boundaries of the lipid membrane. Water molecules are shown in blue (oxygen)/white (hydrogen) stick-ball modus. Lipid molecules are omitted for clarity. Calculations of the root mean square deviation (RMSD) (B) and fluctuation (RMSF) (C) of the Cα atoms. I: traces for Vpu (black, I), CD4 (red, I), BST-2 (blue, I), NTB-A (green, I), A19H (red, II), I3xT (black, II) and W23A (black, III) are shown.

Fig. 1A). The largest distance between the TMDs is recorded for Vpu–Vpu and Vpu–CD4 (12.75 Å). Both dimers adopt large tilts of 12° and −28°, respectively (Table 1, Suppl. Fig. 1B). Dimers with the closest distance are BST-2–BST-2 and Vpu–BST-2 with 9.5 and 9.75 Å, respectively. The former dimer together with I3xT and Vpu–CD4 adopts the largest tilt of + and −28°. The net interaction energy is for BST-2–BST-2 the highest with +4.8 kcal/mol followed by Vpu–Vpu with +2.0 kcal/mol. Values for dimers of Vpu with CD4, BST-2 and NTB-A range from −7.2 to −1.7 kcal/mol.

In the docked lowest energy structure of Vpu–BST-2, BST-2 is positioned so that Leu-11/14/19/23 (green) and Ile-10/15/18 (red) match the alanine rim (Ala-8, Ala-11, Ala-15, Ala-19) of Vpu (Fig. 2A, I). In contrast, Vpu–CD4 shows that CD4 interacts with its Leu-419 (green) and Ile-416 (red) closely with residues of Vpu almost opposite the alanine rim (Fig. 2A, II). NTB-A is oriented so that its Cys-235 (light pink), Phe-238 (yellow), Ile-242 (red) and Leu-243/245/246 (green) also face the Vpu alanine rim (Fig. 2A, III). Embedding these structures into a hydrated lipid bilayer the binding motifs remain unchanged for Vpu–BST-2 and Vpu–CD4 during a 200 ns MD simulation (Fig. 2B, I and II, respectively). The MD simulation of Vpu–NTB-A unravels a movement away from the alanine rim, making the assembly almost similar to the Vpu–CD4 assembly (Fig. 2B, III).

Mutant A19H resembles the binding orientation with BST-2 as in WT in both the docked assembly structure and the structure after MD simulation (Fig. 2A and B, IV, respectively). Residue His-19 is positioned between the two helices interfering with tight and wild type-like packing of the two helices. In VpuI3xT–BST-2, BST-2 is placed in the assembly just on the opposite site of the alanine rim (Fig. 2A and B, V). In Vpu–Vpu one TMD partially blocks the alanine rim in the lowest energy structure after assembly (Fig. 2A, VI). During the simulations the alanine rims of two helices approach each other and one TMD fully blocks the N-terminal part of the rim of the other TMD (Fig. 2B, VI). BST-2–BST-2 shows a tight packing motif (Fig. 2A and B, VII). All other mutants, including RVpu, pack along the mutated alanine rim except for A19L, in which BST-2 packs similar to the motif shown for I3xT (data not shown).

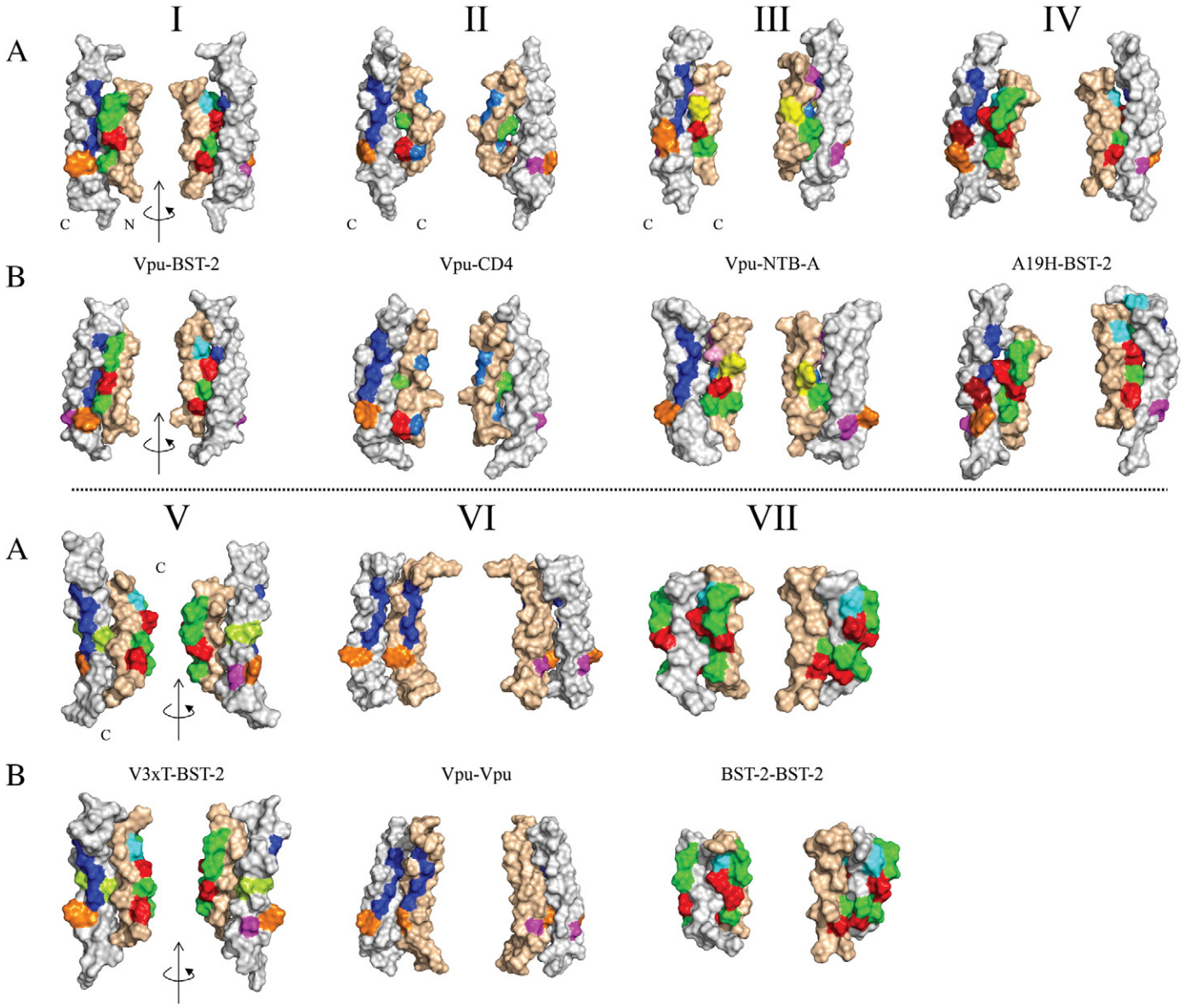

Fig. 2. Graphical representation of the lowest energy dimers from the docking approach (A) and after a 200 ns MD simulations of these lowest energy dimers (B). The following dimers are shown in a surface shape modus as Vpu–BST2 (I), Vpu–CD4 (II), Vpu–NTB-A (III), A18H–BST-2 (IV), I3xT–BST-2 (V), Vpu–Vpu (VI) and BST-2–BST-2 (VII). The following amino acids are shown: alanine (blue), glycine (light blue), leucine (green), isoleucine (red), histidine (dark red), serine (dark pink), cysteine (light pink), threonine (dark green) and phenylalanine (yellow). The structures of the MD simulations are shown without water and lipid molecules. All other residues are shown in white.

3.1. Tilt, kink and distance values over time

Monitoring the distance over time shows that the averaged values for all dimers remain within a range of 9–12 Å and a standard deviation below 1 Å (Table 2). A histogram analysis of the distribution of the distances adopted during the MD simulations reveals that in some dimers the data can be fitted with a single Gaussian (Vpu–CD4, Vpu–NTB-A, Vpu–Vpu, BST-2–BST-2) while in other cases two Gaussians are needed reflecting two adopted positions being screened (Vpu–BST-2, A19H–BST-2, I3xT–BST-2, W23A–BST-2) (Suppl. Fig. 2).

The average tile angle calculated for each of the two helices in each of the simulations ($tilt_{MD}$) spreads considerably (Table 2, Suppl. Fig. 3). In some cases tilts are as large as (33.7 ± 8.1)° (Vpu in I3xT–BST-2) and as low as (7.9 ± 3.5)° (Vpu–Vpu). The differences between the averaged tilt angles calculated over time (Δtilt) are within a range of (18.9 ± 8.3)° (BST-2–BST-2) and (−0.4 ± 5.9)° (Vpu–Vpu) (Table 2). The respective averaged kink angles are calculated as small as (134.5 ± 12.6)° for I3xT in I3xT–BST-2 and as large as (173.5 ± 3.3)° of Vpu in Vpu–NTB-A or Vpu–CD4 (173.2 ± 3.7)°. A histogram analysis of the adopted tilt angles ($tilt_{Histo}$) reveals in some cases up to three positions that are screened using a Gaussian fit to the data (Table 3 and Fig. 3). The bold values in Table 3 indicate those tilt angles which are taken from the largest Gaussian (see Fig. 3). Curve fitting has been limited to a maximal number of 3 Gaussian. The free energy ΔG is calculated from the area spanned by the Gaussian. A correlation between the known biological activity of the dimers and the number of positions screened could not be observed. Estimating the free energy between the positions identifies all of them within a range of 0.5 ± 0.3 kcal/mol (Vpu–Vpu) to 7.8 ± 0.8 kcal/mol (RVpu–CD4) (Table 3). In BST-2–BST-2 the energy is higher (4.1 ±0.4 kcal/mol) compared to the energy necessary to screen different tilt angles in the Vpu–Vpu (1.7 ± 0.5 kcal/mol). The energies follow the sequence Vpu–CD4 (6.7 ± 1.2 kcal/mol) > Vpu–BST2 (3.9 ± 0.3 kcal/mol) > Vpu–NTB-A (2.7 ± 1.0 kcal/mol) for the heterodimers.

Visualizing all the tilt angles from Tables 1 to 3 ($tilt_{MD}$ (Table 2), $tilt_{Histo}$ (Table 3) and $tilt_{MOE}$ (Table 1)) for the dimers investigated

Table 1
Distance ($distance_{MOE}$), tilt ($tilt_{MOE}$), and energy values ($energy_{MOE}$) for the assemblies of the TMDs of Vpu, either as hetero- or homodimers. The total energy and the interface energy are given. The interfacial energy is calculated as the difference between the energy of the respective complex and the energy of the individual structures.

	$distance_{MOE}$ [Å]	$tilt_{MOE}$ [°]	$energy_{MOE}$ [kcal/mol]	interface $energy_{MOE}$ [kcal/mol]
Vpu–BST-2	9.75	0	−586.6	−5.3
Vpu–CD4	12.75	−28	−57.8	−7.2
Vpu–NTB-A	10	4	−774.2	−1.7
A19H–BST-2	11	16	−689.88	−3.2
I3xT–BST-2	10.25	−28	−594.5	−12.8
Vpu–Vpu	12.75	12	−745.5	+2.0
BST-2–BST-2	9.5	28	−343.8	+4.8
W23A–BST-2	11.25	6	−567.6	−6.3
RVpu–BST-2	11.25	−8	−620.4	−12.2
RVpu–CD4	8.5	36	−418.2	−10.6
A19L–BST-2	9.75	−8	−657.7	−10.4
A19N–BST-2	11.5	20	−572.7	−8.1
A19F–BST-2	12.0	4	−621.1	−5.7
A15L–BST-2	10.75	−4	−663.4	−1.1
A15N–BST-2	12	0	−652.5	−5.8
A15F–BST-2	11	24	−620.5	−8.4
I3xV–BST-2	11.5	16	−631.4	−12.7

reveals that the values for the mutants dimers A19H–BST-2 and I3xT–BST-2 are the highest (Fig. 4A). These two mutants abrogate Vpu's capability to induce down-regulation. Vpu–BST-2 has lower values, with Vpu–Vpu showing the lowest values. Taking the Vpu–BST-2 value as the margin, Vpu–CD4 and Vpu–NTB-A adopt values similar to those for Vpu–BST-2 with a tendency of the Vpu–CD4 values being the highest among the three types of heterodimers. All mutant Vpu's investigated show larger values than those for Vpu–BST-2 but not as high as those for A19H–BST-2 and I3xT–BST-2. BST-2–BST-2 and RVpu–BST-2 show also large tilts. The patterns mentioned are independent of the plotted type of tilt angle. Values derived from calculated differences of the individual tilt and kink angles (Δ values) resemble the same pattern in respect to the dimers as mentioned above (Fig. 4B). There is a positive correlation between the tight binding of Vpu to its host partners and the low tilt within the membrane. Abrogation of tight binding results in larger tilts and kink angles adopted at least in one of the TMDs. It is concluded that binding induces a straightening of the helices. The degree of straightening can be used as an analytical tool to predict the binding properties of two helices within the lipid membrane.

4. Discussion

A docking approach is used in combination with MD simulations to derive hetero-dimers [42,43]. The protocol has been validated by assembling the TMDs of M2 into a tetramer and comparing the data with experimentally derived structures [42]. The docking approach is seen as to facilitate the computational handling of the time scales which are found experimentally for the dynamics of membrane proteins and peptides in lipid membranes [47,48].

In this study the structural features are monitored *via* the tilt angles adopted by the homo- and hetero-oligomers. Two analysis pathways are compared, either by simply averaging the tilt and kink angles over the entire simulation or by using the most populated tilt and kink angles adopted during the simulation. In the latter case the population is explored by applying a Gaussian curve fit routine on the histogram analysis of the adopted tilt and kink angles.

A Gaussian fit is seen as an approximation of the distribution of the dynamics of the tilt angle of the TMD. It is assumed that any pose could rather equally tilt in either direction around a mean position, an assumption which may not be necessarily true. Comparing the results using the averaged tilt angle with those calculated from the histogram analysis shows that either value could be used for analysis.

The key feature in this study is that the tilt and consequently the crossing of the two TMDs are based on a docking approach which is independent of the lipids. The data presented show the lowest energy structures. It is anticipated that interaction within the hydrophobic core is highly relevant. Longer segments of the proteins would be necessary to investigate the dependency of the results, here the tilt, on lipid thickness (see [49,50]). Since lipid thickness changes through to the Golgi apparatus the 'proper' conformation and consequently the mode of action could be triggered by lipid thickness [51].

4.1. Relation to experimentally derived structural and functional data

In a cysteine crosslinking study residues on either TMD from Vpu and BST-2 have been identified to be in very close contact [29]. In this study, at the N terminal side Vpu-Ala-7 [Ala-8] links with BST-2-Leu-41 [Leu-23] (see Fig. 3 in [29], values in squared brackets refer to notation in this study) to mention some of the residues which are found to crosslink with each other related to residues. Towards the C terminal side Vpu-Val-21 [Val-22] links with BST-2-Leu-29 [Leu-11] and BST-2-Ile-28 [Ile-10]. Further towards the C terminus, residues Vpu-Val-25/Ile-26/27 [Val-26/Ile-27/28] crosslink with residues BST-2–Leu-24/23

Table 2
Distance ($distance_{MD}$), tilt ($tilt_{MD}$), and kink ($kink_{MD}$) values for the assemblies of the TMDs of Vpu either as hetero- or homodimers. Values are derived from 200 ns MD simulations. The values are given for Vpu and the respective second TMD denoted as 'X', listed in the left column. 'Δ' is the difference value and refers to the blue curves (see e.g. Suppl. Fig. 3 for the Δtilt angles).

MD	$distance_{MD}$ [Å]	$tilt_{MD}$ [°]			$kink_{MD}$ [°]		
		Vpu	X	Δ	Vpu	X	Δ
Vpu–BST-2	9.9 ± 0.7	13.1 ± 5.8	14.7 ± 5.7	−1.6 ± 4.6	169.8 ± 4.3	160.6 ± 5.9	9.2 ± 6.9
Vpu–CD4	10.6 ± 0.4	17.8 ± 4.5	17.2 ± 4.4	0.6 ± 3.6	173.2 ± 3.7	167.8 ± 5.2	5.4 ± 5.8
Vpu–NTB-A	10.6 ± 0.3	12.5 ± 6.0	9.8 ± 4.6	2.7 ± 3.9	173.5 ± 3.3	171.4 ± 4.2	2.1 ± 4.9
A19H–BST-2	10.7 ± 0.1	19.5 ± 7.2	33.0 ± 2.2	−13.5 ± 6.4	162.6 ± 6.9	162.0 ± 5.5	0.5 ± 7.7
I3xT–BST-2	9.9 ± 0.07	33.7 ± 8.1	22.3 ± 6.1	11.3 ± 4.5	134.5 ± 12.6	160.7 ± 8.6	26.2 ± 10.8
Vpu–Vpu	10.9 ± 0.04	7.9 ± 3.5	8.3 ± 4.9	−0.4 ± 5.9	166.5 ± 5.1	164.6 ± 4.1	1.9 ± 6.1
BST-2–BST-2	9.2 ± 0.04	29.5 ± 5.3	10.6 ± 4.3	18.9 ± 8.3	145.0 ± 8.3	167.1 ± 6.2	−22.0 ± 12.3
W23A–BST-2	11.6 ± 0.07	17.9 ± 5.4	19.7 ± 5.1	−1.8 ± 5.7	169.7 ± 5.2	169.7 ± 5.6	−0.04 ± 8.1
RVpu–BST-2	10.5 ± 0.1	21.3 ± 3.6	19.9 ± 4.7	1.3 ± 4.9	160.6 ± 5.9	165.5 ± 5.1	−4.9 ± 8.1
RVpu–CD4	9.2 ± 0.0	11.6 ± 4.7	17.8 ± 5.5	−6.3 ± 8.5	161.7 ± 5.8	172.6 ± 4.8	−10.9 ± 6.7
A19L–BST-2	12.7 ± 0.09	15.9 ± 5.8	10.1 ± 4.8	5.8 ± 4.6	158.5 ± 9.1	169.5 ± 5.8	−11.1 ± 10.7
A19N–BST-2	10.9 ± 0.0	11.2 ± 4.4	19.3 ± 6.9	−8.1 ± 7.8	164.1 ± 4.4	160.1 ± 8.9	3.9 ± 10.3
A19F–BST-2	10.7 ± 0.1	16.3 ± 4.3	10.2 ± 4.0	6.1 ± 3.8	168.6 ± 4.4	170.8 ± 5.0	−2.2 ± 6.7
A15L–BST-2	11.6 ± 0.1	8.1 ± 3.9	9.9 ± 5.5	−1.8 ± 6.1	163.9 ± 4.8	159.5 ± 9.1	4.5 ± 10.0
A15N–BST-2	9.0 ± 0.0	16.7 ± 4.6	26.2 ± 5.4	−9.4 ± 4.3	168.5 ± 3.9	159.6 ± 7.1	8.9 ± 7.5
A15F–BST-2	10.0 ± 0.1	12.3 ± 6.4	8.5 ± 4.3	3.8 ± 7.8	166.3 ± 4.7	168.6 ± 6.1	−1.9 ± 7.5
I3xV–BST-2	11.3 ± 0.1	8.5 ± 3.8	12.2 ± 5.0	−3.6 ± 5.8	173.3 ± 3.6	162.4 ± 5.7	10.9 ± 7.0

Table 3
Tilt ($tilt_{Histo}$), the respective difference tilt ($\Delta tilt_{Histo}$) and energy values for the dimers of Vpu either as hetero- or homodimers. The values are derived from a histogram analysis and curve fitting (Gaussian fit). The bold values indicate those tilt angles which are taken from the largest Gaussian (see Fig. 3). Curve fitting has been limited to a maximal number of 3 Gaussian. The free energy ΔG is calculated from the area spanned by the Gaussian. Negative signs are put in brackets since as such the direction of the tilt is not further considered. 'Δ' refers to the Gaussian calculated from the histogram of the Δ-values from the MD simulations. In the case of three $tilt_{Histo}$ values, the ΔG values in the first line refer to calculations with the first two $tilt_{Histo}$ values and the values in the second line refer to calculations with the second and third $tilt_{Histo}$ values.

	$Tilt_{Histo}$ [°]	$Tilt_{Histo}$ [°]	$Tilt_{Histo}$ [°]	ΔG [kJ/mol]	$\Delta Tilt_{Histo}$ [°]	$\Delta Tilt_{Histo}$ [°]	ΔG [kJ/mol]
Vpu–BST-2	**11.3 ± 4.2**	20.9		−3.9 ± 0.3	**(−)2.1 ± 3.9**		
	12.4 ± 4.0	20.8		−2.4 ± 0.4			
Vpu–CD4	25.5	**18.2 ± 3.5**	13.0	6.7 ± 1.2	**1.3 ± 2.6**		
				−4.4 ± 1.4			
	18.5 ± 3.4	13.0		−3.9 ± 0.8			
Vpu–NTB-A	6.4	**13.9 ± 2.8**	21.6	0.6 ± 1.0	**3.2 ± 3.1**		
				−2.7 ± 1.0			
	8.6	**15.4 ± 4.9**		−4.0 ± 4.1			
A19H–BST-2	20.1	**36.9 ± 3.8**		4.4 ± 0.2	**10.5 ± 1.8**	16.2	2.3 ± 0.1
	8.9	**22.7 ± 2.7**	29.7	−4.8 ± 0.1			
				4.0 ± 0.1			
I3xT–BST-2	**13.9 ± 4.2**	26.1		−0.6 ± 0.6	**(−)11.5 ± 4.2**	(−)25.5	8.1 ± 0.4
	36.5	**32.1 ± 3.4**		2.7 ± 0.9			
Vpu–Vpu	**5.5 ± 2.1**	10.7		−0.5 ± 0.3	**(−)2.9 ± 5.0**	4.8	−1.9 ± 0.2
	5.8 ± 2.4	13.0		−1.7 ± 0.5			
BST-2–BST-2	29.3	**29.8 ± 2.0**		4.1 ± 0.4	1.7	**20.3 ± 6.4**	6.9 ± 0.4
	11.7 ± 3.6	6.4		−3.5 ± 1.2			
W23A–BST-2	10.6	**20.4 ± 3.2**		3.5 ± 1.7	**(−)3.7 ± 5.1**	0.6	0.5 ± 1.2
	4.1	**18.2 ± 3.6**	22.6	6.2 ± 0.2			
				−4.1 ± 0.4			
RVpu–BST-2	15.5	**22.2 ± 2.5**		5.1 ± 0.2	**1.1 ± 4.2**		
	18.0 ± 3.5	24.2		−1.9 ± 0.7			
RVpu–CD4	12.3	**11.4 ± 4.4**		7.8 ± 0.8	**0.1 ± 6.0**	(−)11.5	−0.5 ± 0.6
	12.5	**18.5 ± 4.8**		5.8 ± 0.4			
A19L–BST-2	8.1	**18.6 ± 3.2**		2.8 ± 0.1	**5.9 ± 3.4**	10.3	
	13.1 ± 3.0	5.0		−1.3 ± 0.2			
A19N–BST-2	7.4	**13.3 ± 3.4**		1.7 ± 0.3	**(−)8.3 ± 6.7**		
	18.2 ± 4.6	33.8		−6.3 ± 0.2			
A19F–BST-2	4.4	**10.8 ± 1.6**	16.9	1.9 ± 0.9	**6.3 ± 3.2**		
				7.1 ± 0.7			
	9.7 ± 3.2						
A15L–BST-2	**9.9 ± 3.0**	20.1		−2.9 ± 1.0	**(−)0.5 ± 3.7**	(−)13.9	−5.6 ± 0.4
	7.8 ± 3.4	19.1		−4.0 ± 0.1			
A15N–BST-2	**17.1 ± 3.9**				**(−)9.5 ± 3.6**		
	22.9	**29.3 ± 2.9**		0.6 ± 0.3			
A15F–BST-2	**9.7 ± 3.9**	20.1		−2.9 ± 1.0	**(−)1.0 ± 4.9**	10.4	−0.8 ± 0.3
	3.9	**9.8 ± 3.3**		3.0 ± 0.3			
I3xV–BST-2	5.0	**9.9 ± 3.0**		2.5 ± 0.8	**0.9 ± 3.0**	(−)8.3	0.0 ± 0.1
	5.1	**12.5 ± 4.4**		7.6 ± 0.5			

[Leu-5/6], but do not match findings in this study. This lack of matching could be due to the fact that for the reported residues full-length proteins have been used. The missing information about interacting partners within the core of the bilayer is eventually related to the non-accessibility of the site by the reagents [29].

Evidence for the role of tilt angles on experimental data has been reported [35]. Mutations within the TMD of BST-2 induce strong tilts based on NMR spectroscopic experiments [35]. These mutations are reported to escape down modulation *in vivo*. The tilt angles of Vpu have been reported to be 28° independent of the presence of BST-2. An angle of 21° has been measured for solely BST-2, 24° in the presence of Vpu. Thus, antiparallel Vpu–BST-2 leads to an increased tilt of one of the partners, here BST-2, with the consequence of lowering the difference between the two TMDs. In an effort to synchronize the data of this study with those from the experiments, despite the differences in the experimental set-ups in respect to amino acid sequence and lipids used, it is stressed that the Δtilt values for Vpu–BST-2 are low. The values for Vpu–Vpu are in the same range, whereas those of BST-2–BST-2 are larger than the values for Vpu–BST2. The large values for BST-2–BST-2 are rather lowest energy structures, and it is possible that these tilts cannot be adopted in the experiments. Thus, it is rather proposed that the NMR data in respect to BST-2 represent most likely loosely assembled peptides. Only minimal chemical shift changes are reported for the triple mutant Vpu-AAA/FFF when measured in the presence of BST-2. The data are interpreted as a weak binding between two TMDs. According to the present study, larger tilts should be expected. The NMR data further confirm the important role of the alanine rim in Vpu–BST-2 binding.

The mutants used in this study are all chosen based on available experimental data on these mutants. A comparison of the activity of Vpu A19N and A15N to down-regulate BST-2 shows slightly higher activity for the latter (Fig. 1, C and E in [11]). The findings corroborate the presented data in this study: comparison of A19N–BST-2 and A15N–BST-2 reveals that the latter is screening a larger tilt at least for one of the TMDs than A19N–BST-2. A19H–BST-2 adopts larger tilt angles than W23A–BST-2, which appears parallel with the same trend in BST-2 down regulation [10]. Comparison of Vpu–BST-2 and W23A–BST-2 tilt angles of this study (tilt 11.3/12.4° of Vpu–BST-2 < 20.4/18.2° of W23A–BST-2) reveals that the values can be correlated with the experimental data for monitoring particle release, which is about 50–60% lower for the mutant than for WT [35]. A15F–BST-2 and A15L–BST-2 compared with W23A behave in this study similar than in the experimental study [35,52] with the former two being less active than the latter. A triple mutation of Ile-15, Ile-16 and Ile-17 each into

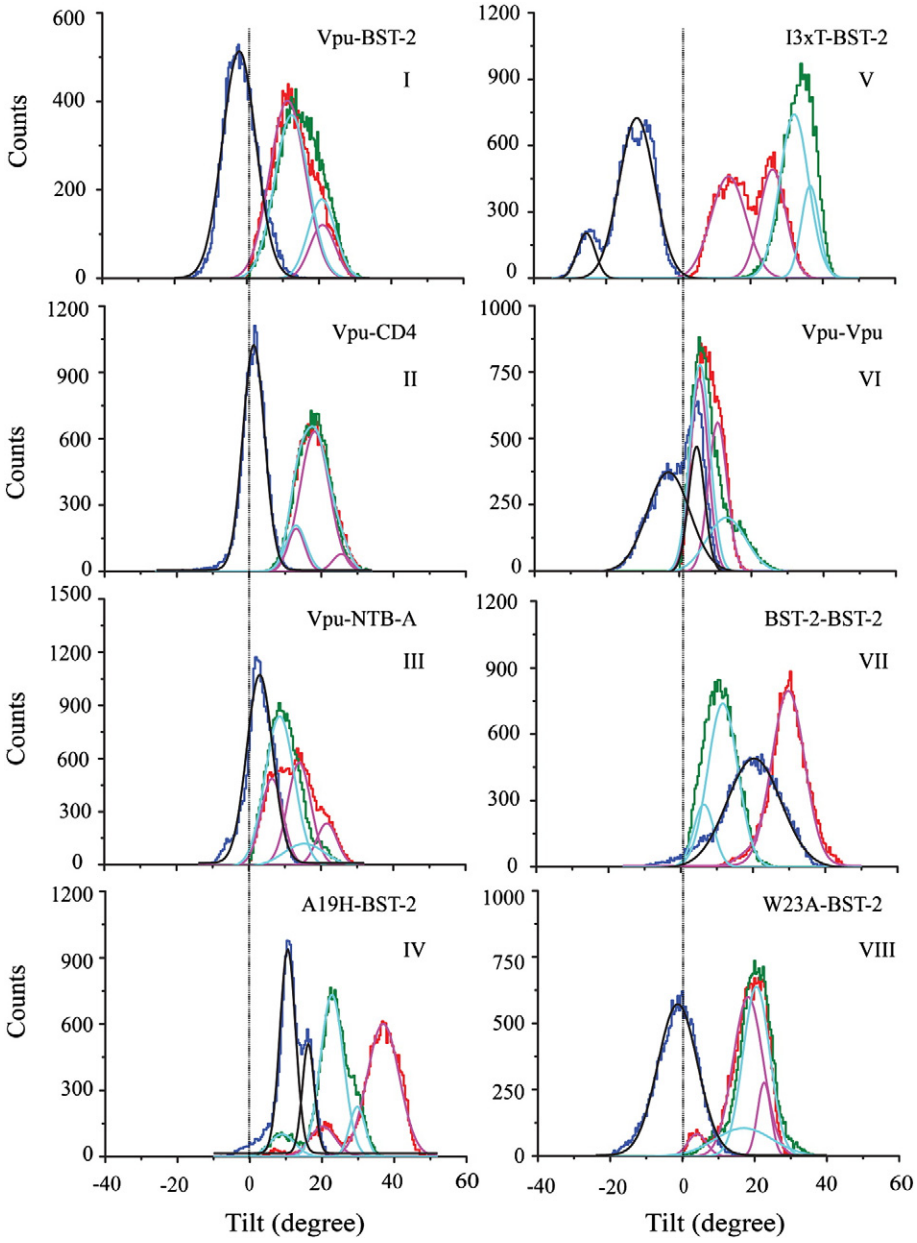

Fig. 3. Histogram analysis of the tilt angles calculated from 200 ns MD simulations for Vpu–BST-2 (I), Vpu–CD4 (II), Vpu–NTB-A (III), A19H–BST-2 (IV), I3xT–BST-2 (V), Vpu–Vpu (VI), BST-2–BST-2 (VII) and W23A–BST-2 (VIII). The angles for Vpu are shown in red, those for the other TMDs in green. The difference between the two tilt angles (Δtilt) is shown in blue. The respective Gaussian fits are shown in light red (Vpu) and light blue (other TMDs) and black (Δtilt).

threonine has found to abrogate the interaction of the Vpu mutant with BST-2 [53]. In the data presented here, it is found that, I3xT leads to a large alteration of the tilt angle compared to WT data.

Full length Vpu with a randomized sequence of the TMD is able to induce CD4 degradation [22]. Thus, RVpu–CD4 serves as a 'control' regarding the Vpu–CD4 data. The data set for RVpu–BST-2 and Vpu–BST-2 is almost similar to the data set for RVpu–CD4/Vpu–CD4. There is a slight trend for the tilt in the RVpu–BST-2 dimer to be larger than in the Vpu–BST-2 dimer, suggesting that the RVpu–BST-2 interaction and activity should be less than that for Vpu–BST-2.

4.2. Predictions — Vpu with BST-2, and with CD4 or NTB-A

Structural features of the dimers indicate that BST-2 binds with isoleucine/leucine residues within its TMD to the alanine rim of Vpu [35,54]. Any distortion of this binding site reduces interaction activity. The loss of the interaction appears to correlate with larger tilts and kinks of the helices within the dimer complex in the lipid membrane.

Vpu–BST-2 and Vpu–NTB-A show marginal smaller tilt angles and energies between different positions than Vpu–CD4, but all three of them show larger tilt and energy values than Vpu–Vpu. Vpu–CD4 should have the lowest degree of interaction. Experimentally it has been shown that the TMD of Vpu is dispensable for CD4 down-regulation and that it is rather an interaction within the cytoplasmic domain of Vpu which is responsible for the interaction [11]. Thus, higher values than those for Vpu–Vpu and its dimers with BST-2 and NTB-A are reasonable. In respect to BST-2, it is still a debate whether Vpu is co-down-regulated. According to this study the tilt is low, which could be interpreted that there would be some chance for co-down-regulation. The same stands for the interaction of Vpu with NTB-A, Vpu retains

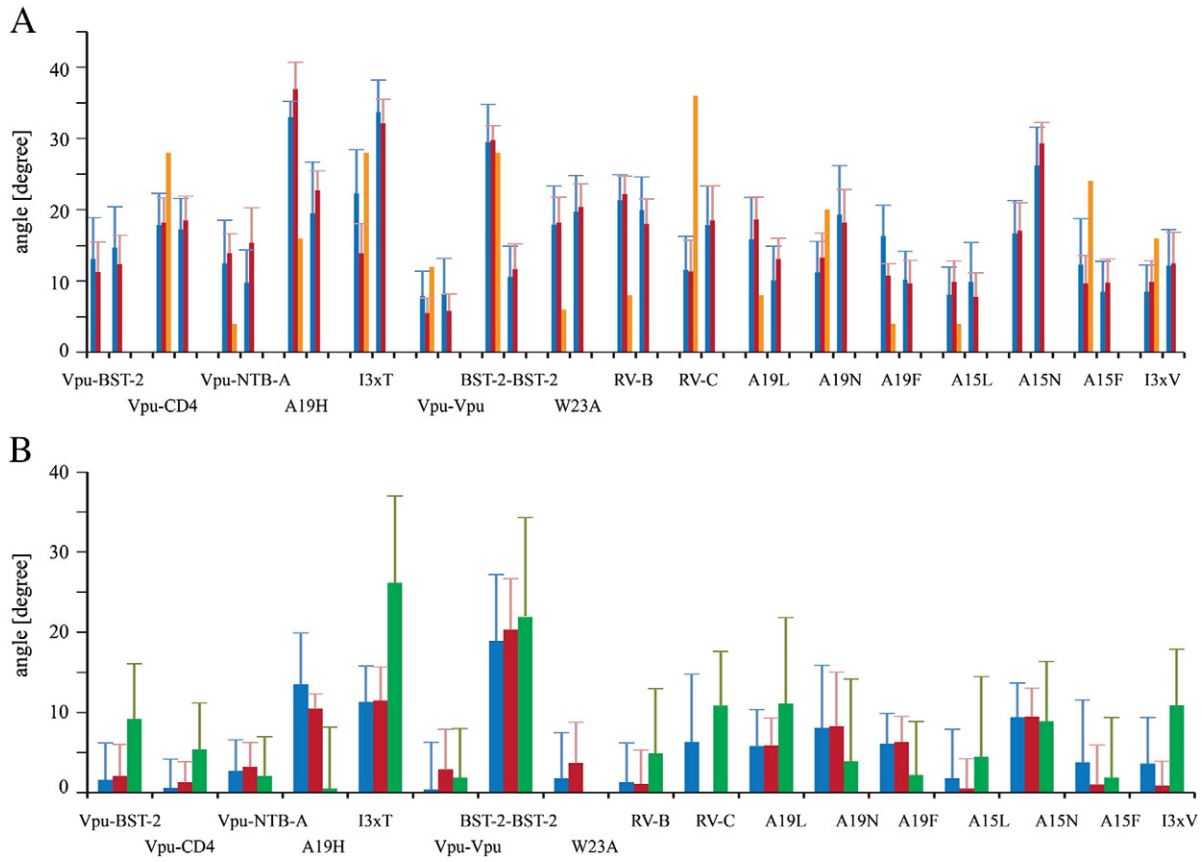

Fig. 4. Visualization of the different tilt angles $tilt_{MD}$ (blue), $tilt_{Histo}$ (red), and $tilt_{MOE}$ (orange) taken from the tables (A). For a set of columns, the first of two bars for each dimer (blue and red) represents values for Vpu (and its mutants), the second set of two bars (blue and red) represents the corresponding TMDs. The calculated difference values between the individual tilts of the two TMDs are shown as $\Delta tilt_{MD}$ (blue) and $\Delta tilt_{Histo}$ (red) as well as the difference in the kink angles ($\Delta kink_{MD}$, green) (B). The dimers are from left to right Vpu–BST-2, Vpu–CD4, Vpu–NTB-A, A18H–BST-2 (A18H), I3xT–BST-2 (I3xT), Vpu–Vpu, BST-2–BST-2, W23A–BST-2 (W23A), RVpu–BST-2 (RV-B), RVpu–CD4 (RV-C), A19L–BST-2 (A19L), A19N–BST-2 (A19N), A19F–BST-2 (A19F), A15L–BST-2 (A15L), A15N–BST-2 (A15N), A15F–BST-2 (A15F), and I3xV–BST-2 (I3xV).

NTB-A within the Golgi apparatus and affects the glycosylation pattern of NTB-A [28,55]. Thus, a tight binding similar to the Vpu–BST-2 binding could be possible.

BST-2 is found to be a dimer [56]. According to the tilt angle analysis the large values would support experimental findings, and that dimerization should not be driven by the TMD but rather by its ectodomain [54].

Vpu's activity within the lipid membrane depends on the dynamics it shows with the host target. MD simulations are used as an analytical tool to address the dynamics of the TMDs and to describe the correlation between the adopted tilt and the biological interaction activity of the proteins. Tight binding, or irreversible binding is shown by screening an almost parallel alignment. If the alignment becomes less parallel the interaction activity is lower. If the biological activity requires tight binding, 'crossed' TMDs should not show an optimum biological activity. With the alanine rim as the potential binding site the binding pose is supposed to be a fairly straight alignment of the two helices.

5. Conclusions

The alanine rim is considered to be an important host binding site. Monitoring the dynamics of the tilt angle between two helices can be used for predicting not only the activity but also the degree of the activity. Classical MD simulations in combination with docking approaches can be used to identify potential binding motifs within the lipid membrane. The data suggest the protocol to be a highly potential tool in computational bioanalytics to screen target-host interactions of membrane proteins focusing on their TMDs.

Acknowledgement

We thank J. Guatelli (San Diego, USA) for the stimulating and valuable discussions. Thanks also to Meng-Han Lin and Roman Schilling for supportive discussions. WBF thanks the NYMU, the government of Taiwan for financial support (Aim of Excellence Program). This work was also supported by the National Science Council of Taiwan (NSC98-2112-M-010-002-MY3). We acknowledge the National Center for High-Performance Computing (NCHC), TW, for providing computer time and service.

Appendix A. Supplementary data

Supplementary data to this article can be found online at http://dx.doi.org/10.1016/j.bbamem.2013.07.032.

References

[1] W.B. Fischer, Y.-T. Wang, C. Schindler, C.-P. Chen, Mechanism of function of viral channel proteins and implications for drug development, Int. Rev. Cell Mol. Biol. 294 (2012) 259–321.
[2] J.L. Nieva, V. Madan, L. Carrasco, Viroporins: structure and biological functions, Nat. Rev. Microbiol. 10 (2012) 563–574.
[3] M. Neupärtl, C. Meyer, I. Woll, F. Frohns, M. Kang, J.L. Van Etten, D. Kramer, B. Hertel, A. Moroni, G. Thiel, Chlorella viruses evoke a rapid release of K^+ from host cells during the early phase of infection, Virology 372 (2008) 340–348.
[4] W.B. Fischer, J. Krüger, Viral channel forming proteins, Int. Rev. Cell Mol. Biol. 275 (2009) 35–63.
[5] F. Ciampor, P.M. Bayley, M.V. Nermut, E.M. Hirst, R.J. Sugrue, A.J. Hay, Evidence that the amantadine-induced, M_2-mediated conversion of influenza A virus

hemagglutinin to the low pH conformation occurs in an acidic *trans* Golgi compartment, Virology 188 (1992) 14–24.
[6] R.J. Sugrue, G. Bahadur, M.C. Zambon, M. Hall-Smith, A.R. Douglas, A.J. Hay, Specific structural alteration of the influenza haemagglutinin by amantadine, EMBO J. 9 (1990) 3469–3476.
[7] L.F. Wetherill, K.K. Holmes, M. Verow, M. Müller, G. Howell, M. Harris, C. Fishwick, N. Stonehouse, R. Foster, G.E. Blair, S. Griffin, A. Macdonald, High-risk human papillomavirus E5 oncoprotein displays channel-forming activity sensitive to small-molecule inhibitors, J. Virol. 86 (2012) 5341–5351.
[8] M. Conrad, V.J. Bubb, R. Schlegel, The human papillomavirus type 6 and 16 E5 proteins are membrane-associated proteins which associate with the 16-kilodalton pore-forming protein, J. Virol. 67 (1993) 6170–6178.
[9] G. Cui, C. Fang, K. Han, Prediction of protein–protein interactions between viruses and human by an SVM model, BMC Bioinforma. 13 (2012) S5.
[10] M. Skasko, A. Tokarev, C.-C. Chen, W.B. Fischer, S.K. Pillai, J. Guatelli, BST-2 is rapidly down-regulated from the cell surface by the HIV-1 protein Vpu: evidence for a post-ER mechanism of Vpu-action, Virology 411 (2011) 65–77.
[11] S. Bolduan, J. Votteler, V. Lodermeyer, T. Greiner, H. Koppensteiner, M. Schindler, G. Thiel, U. Schubert, Ion channel activity of HIV-1 Vpu is dispensable for counteraction of CD317, Virology 416 (2011) 75–85.
[12] K. Strebel, T. Klimkait, M.A. Martin, Novel gene of HIV-1, *vpu*, and its 16-kilodalton product, Science 241 (1988) 1221–1223.
[13] E.A. Cohen, E.F. Terwilliger, J.G. Sodroski, W.A. Haseltine, Identification of a protein encoded by the *vpu* gene of HIV-1, Nature 334 (1988) 532–534.
[14] T. Huet, R. Cheynier, A. Meyerhans, G. Roelants, Genetic organization of a chimpanzee lentivirus related to HIV-1, Nature 345 (1990) 356–359.
[15] T. Klimkait, K. Strebel, M.D. Hoggan, M.A. Martin, J.M. Orenstein, The human immunodeficiency virus type 1-specific protein vpu is required for efficient virus maturation and release, J. Virol. 64 (1990) 621–629.
[16] R.H. Miller, N. Sarver, HIV accessory proteins as therapeutic targets, Nat. Med. 3 (1997) 389–394.
[17] M.H. Malim, M. Emerman, HIV-1 accessory proteins — ensuring viral survival in a hostile environment, Cell Host Microbe 3 (2008) 388–398.
[18] W.C. Greene, B.M. Peterlin, Charting HIV's remarkable voyage through the cell: basic science as a passport to future therapy, Nat. Med. 8 (2002) 673–680.
[19] F. Maldarelli, M.Y. Chen, R.L. Willey, K. Strebel, Human-immunodeficiency-virus type-1 Vpu protein is an oligomeric type-I integral membrane protein, J. Virol. 67 (1993) 5056–5061.
[20] A. Hussain, S.R. Das, C. Tanwar, S. Jameel, Oligomerization of the human immunodeficiency virus type I (HIV-1) Vpu protein — a genetic, biochemical and biophysical analysis, Virol. J. 4 (2007) 1–11.
[21] J.-X. Lu, S. Sharpe, R. Ghirlando, W.-M. Yau, R. Tycko, Oligomerization state and supramolecular structure of the HIV-1 Vpu protein transmembrane segment in phospholipid bilayers, Prot. Sci. 19 (2010) 1877–1896.
[22] U. Schubert, A.V. Ferrer-Montiel, M. Oblatt-Montal, P. Henklein, K. Strebel, M. Montal, Identification of an ion channel activity of the Vpu transmembrane domain and its involvement in the regulation of virus release from HIV-1-infected cells, FEBS Lett. 398 (1996) 12–18.
[23] U. Schubert, S. Bour, A.V. Ferrer-Montiel, M. Montal, F. Maldarelli, K. Strebel, The two biological activities of human immunodeficiency virus type 1 Vpu protein involve two separable structural domains, J. Virol. 70 (1996) 809–819.
[24] N. van Damme, D. Goff, C. Katsura, R.L. Jorgensen, R. Mitchell, M.C. Johnson, E.B. Stephens, J. Guatelli, The interferon-induced protein BST-2 restricts HIV-1 release and is downregulated from the cell surface by the viral Vpu protein, Cell Host Microbe 3 (2008) 1–8.
[25] S.J.D. Neil, T. Zang, P.D. Bieniasz, Tetherin inhibits retrovirus release and is antagonized by HIV-1 Vpu, Nature 451 (2008) 425–431.
[26] S.F. Kluge, D. Sauter, M. Vogl, M. Peeters, Y. Li, F. Bibollet-Ruche, B.H. Hahn, F. Kirchhoff, The transmembrane domain of HIV-1 Vpu is sufficient to confer anti-tetherin activity to SIVcpz and SIVgor Vpu proteins: cytoplasmic determinants of Vpu function, Retrovirology 10 (2013) 32.
[27] A. Hussain, C. Wesley, M. Khalid, A. Chaudhry, S. Jameel, Human immunodeficiency virus type 1 Vpu protein interacts with CD74 and modulates major histocompatibility complex class II presentation, J. Virol. 82 (2008) 893–902.
[28] A.H. Shah, B. Sowrirajan, Z.B. Davis, J.P. Ward, E.M. Campbell, V. Planelles, E. Barker, Degranulation of natural killer cells following interaction with HIV-1-infected cells is hindered by downmodulation of NTB-A by Vpu, Cell Host Microbe 8 (2010) 397–409.
[29] M.W. McNatt, T. Zang, P.D. Bieniasz, Vpu binds directly to tetherin and displaces it from nascent virions, PLoS Pathog. 9 (2013) e1003299.
[30] F.M. Marassi, C. Ma, H. Gratkowski, S.K. Straus, K. Strebel, M. Oblatt-Montal, M. Montal, S.J. Opella, Correlation of the structural and functional domains in the membrane protein Vpu from HIV-1, Proc. Natl. Acad. Sci. U. S. A. 96 (1999) 14336–14341.
[31] V. Wray, R. Kinder, T. Federau, P. Henklein, B. Bechinger, U. Schubert, Solution structure and orientation of the transmembrane anchor domain of the HIV-1-encoded virus protein U by high resolution and solid-state NMR spectroscopy, Biochemistry 38 (1999) 5272–5282.
[32] P. Henklein, R. Kinder, U. Schubert, B. Bechinger, Membrane interactions and alignment of structures within the HIV-1 Vpu cytoplasmic domain: effect of phosphorylation of serines 52 and 56, FEBS Lett. 482 (2000) 220–224.
[33] S.H. Park, A.A. Mrse, A.A. Nevzorov, M.F. Mesleh, M. Oblatt-Montal, M. Montal, S.J. Opella, Three-dimensional structure of the channel-forming trans-membrane domain of virus protein "u" (Vpu) from HIV-1, J. Mol. Biol. 333 (2003) 409–424.
[34] J. Krüger, W.B. Fischer, Exploring the conformational space of Vpu from HIV-1: a versatile and adaptable protein, J. Comput. Chem. 29 (2008) 2416–2424.
[35] M. Skasko, Y. Wang, Y. Tian, A. Tokarev, J. Munguia, A. Ruiz, E.B. Stephens, S.J. Opella, J. Guatelli, HIV-1 Vpu protein antagonizes the innate restriction factor BST-2 via lipid-embedded helix-helix interactions, J. Biol. Chem. 287 (2012) 58–67.
[36] W.B. Fischer, H.J. Hsu, Viral channel forming proteins — modelling the target, Biochim. Biophys. Acta 1808 (2011) 561–571.
[37] D. Langosch, I.T. Arkin, Interaction and conformational dynamics of membrane-spanning protein helices, Protein Sci. 18 (2009) 1343–1358.
[38] A. Fink, N. Sal-Man, D. Gerber, Y. Shai, Transmembrane domains interactions within the membrane milieu: principles, advances and challenges, Biochim. Biophys. Acta 1818 (2012) 974–983.
[39] A. Kukol, P.D. Adams, L.M. Rice, A.T. Brunger, I.T. Arkin, Experimentally based orientational refinement of membrane protein models: a structure for the influenza A M2 H^+ channel, J. Mol. Biol. 286 (1999) 951–962.
[40] A.J. Beevers, A. Kukol, Systematic molecular dynamics searching in a lipid bilayer: application to the glycophorin A and oncogenic ErbB-2 transmembrane domains, J. Mol. Graph. Model. 25 (2006) 226–233.
[41] L. Bu, W. Im, C.L. Brooks III, Membrane assembly of simple helix homo-oligomers studied via molecular dynamics simulations, Biophys. J. 92 (2007) 854–863.
[42] J. Krüger, W.B. Fischer, Assembly of viral membrane proteins, J. Chem. Theory Comput. 5 (2009) 2503–2513.
[43] H.-J. Hsu, W.B. Fischer, In silico investigations of possible routes of assembly of ORF 3a from SARS-CoV, J. Mol. Model. 18 (2011) 501–514.
[44] M. Heyden, J.A. Freites, M.B. Ulmschneider, S.H. White, D.J. Tobias, Assembly and stability of α-helical membrane proteins, Soft Matter 8 (2012) 7742–7752.
[45] T. Kim, W. Im, Revisiting hydrophobic mismatch with free energy simulation studies of transmembrane helix tilt and rotation, Biophys. J. 99 (2010) 175–183.
[46] J.E. Goose, M.S.P. Sansom, Reduced lateral mobility of lipids and proteins in crowded membranes, PLoS Comput. Biol. 9 (2013) e1003033.
[47] M. Vrljic, S.Y. Nishimura, S. Brasselet, W.E. Moerner, H.M. McConnell, Translational diffusion of individual class II MHC membrane proteins in cells, Biophys. J. 83 (2002) 2681–2692.
[48] S. Ramadurai, A. Holt, L.V. Schäfer, V.V. Krasnicov, D.T.S. Rijkers, S.J. Marrink, J.A. Killian, B. Poolman, Influence of hydrophobic mismatch and amino acid composition on the lateral diffusion of transmembrane peptides, Biophys. J. 99 (2010) 1447–1454.
[49] S.H. Park, S.J. Opella, Tilt angle of a trans-membrane helix is determined by hydrophobic mismatch, J. Mol. Biol. 350 (2005) 310–318.
[50] Y.-H. Lam, S.R. Wassall, C.J. Morton, R. Smith, F. Separovic, Solid-state NMR structure determination of melittin in a lipid environment, Biophys. J. 81 (2011) 2752–2761.
[51] T. Mehnert, A. Routh, P.J. Judge, Y.H. Lam, D. Fischer, A. Watts, W.B. Fischer, Biophysical characterisation of Vpu from HIV-1 suggests a channel-pore dualism, Proteins 70 (2008) 1488–1497.
[52] R. Vigan, S.J.D. Neil, Determinants of tetherin antagonism in the transmembrane domain of the human immunodeficiency virus type 1 Vpu protein, J. Virol. 84 (2010) 12958–12970.
[53] M. Lv, J. Wang, T. Zuo, Y. Zhu, W. Kong, X. Yu, Polarity changes in the transmembrane domain core of HIV-1 Vpu inhibits anti-tetherin activity, PLoS One 6 (2011) e20890.
[54] T. Kobayashi, H. Ode, T. Yoshida, K. Sato, P. Gee, S.P. Yamamoto, H. Ebina, K. Strebel, H. Sato, Y. Koyanagi, Identification of amino acids in the human tetherin transmembrane domain responsible for HIV-1 Vpu interaction and susceptibility, J. Virol. 85 (2011) 932–945.
[55] S. Bolduan, P. Hubel, T. Reif, V. Lodermeyer, K. Höhne, J.V. Fritz, D. Sauter, F. Kirchhoff, O.T. Fackler, M. Schindler, U. Schubert, HIV-1 Vpu affects the anterograde transport and the glycosylation pattern of NTB-A, Virology 440 (2013) 190–203.
[56] T. Ohtomo, Y. Sugamata, Y. Ozaki, K. Ono, Y. Yoshimura, S. Kawai, Y. Koishihara, S. Ozaki, M. Kosaka, T. Hirano, M. Tsuchiya, Molecular cloning and characterization of a surface antigen preferentially overexpressed on multiple myeloma cells, Biochem. Biophys. Res. Commun. 258 (1999) 583–591.